



Aalborg Universitet

AALBORG UNIVERSITY  
DENMARK

## HypoxamiR-210 accelerates wound healing in diabetic mice by improving cellular metabolism

Narayanan, Sampath; Eliasson Angelstig, Sofie; Xu, Cheng; Grünler, Jacob; Zhao, Allan; Zhu, Wan; Xu Landén, Ning; Ståhle, Mona; Zhang, Jingping; Ivan, Mircea; Maltesen, Raluca Georgiana; Botusan, Ileana Ruxandra; Rajamand Ekberg, Neda; Zheng, Xiaowei; Catrina, Sergiu-Bogdan

*Published in:*  
Communications Biology

*DOI (link to publication from Publisher):*  
[10.1038/s42003-020-01495-y](https://doi.org/10.1038/s42003-020-01495-y)

*Creative Commons License*  
CC BY 4.0

*Publication date:*  
2020

*Document Version*  
Publisher's PDF, also known as Version of record

[Link to publication from Aalborg University](#)

### *Citation for published version (APA):*





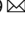


Narayanan, S., Eliasson Angelstig, S., Xu, C., Grünler, J., Zhao, A., Zhu, W., Xu Landén, N., Ståhle, M., Zhang, J., Ivan, M., Maltesen, R. G., Botusan, I. R., Rajamand Ekberg, N., Zheng, X., & Catrina, S-B. (2020). HypoxamiR-210 accelerates wound healing in diabetic mice by improving cellular metabolism. *Communications Biology*, 3(1), [768]. <https://doi.org/10.1038/s42003-020-01495-y>

### **General rights**

Copyright and moral rights for the publications made accessible in the public portal are retained by the authors and/or other copyright owners and it is a condition of accessing publications that users recognise and abide by the legal requirements associated with these rights.

- ? Users may download and print one copy of any publication from the public portal for the purpose of private study or research.
- ? You may not further distribute the material or use it for any profit-making activity or commercial gain
- ? You may freely distribute the URL identifying the publication in the public portal ?

## HypoxamiR-210 accelerates wound healing in diabetic mice by improving cellular metabolism

Sampath Narayanan<sup>1,2</sup>, Sofie Eliasson Angelstig<sup>1,2</sup>, Cheng Xu<sup>1,2</sup>, Jacob Grünler<sup>1,2</sup>, Allan Zhao<sup>1</sup>, Wan Zhu<sup>3</sup>, Ning Xu Landén <sup>4</sup>, Mona Ståhle<sup>4</sup>, Jingping Zhang<sup>5</sup>, Mircea Ivan <sup>6</sup>, Raluca Georgiana Maltesen <sup>7</sup>, Ileana Ruxandra Botusan<sup>1,2</sup>, Neda Rajamand Ekberg<sup>1,2</sup>, Xiaowei Zheng <sup>1,2,9</sup>  & Sergiu-Bogdan Catrina <sup>1,2,8,9</sup> 

Wound healing is a high energy demanding process that needs a good coordination of the mitochondria with glycolysis in the characteristic highly hypoxic environment. In diabetes, hyperglycemia impairs the adaptive responses to hypoxia with profound negative effects on different cellular compartments of wound healing. miR-210 is a hypoxia-induced microRNA that regulates cellular metabolism and processes important for wound healing. Here, we show that hyperglycemia blunted the hypoxia-dependent induction of miR-210 both in vitro and in human and mouse diabetic wounds. The impaired regulation of miR-210 in diabetic wounds is pathogenic, since local miR-210 administration accelerated wound healing specifically in diabetic but not in non-diabetic mice. miR-210 reconstitution restores the metabolic balance in diabetic wounds by reducing oxygen consumption rate and ROS production and by activating glycolysis with positive consequences on cellular migration. In conclusion, miR-210 accelerates wound healing specifically in diabetes through improvement of the cellular metabolism.

<sup>1</sup>Department of Molecular Medicine and Surgery, Karolinska Institutet, Stockholm, Sweden. <sup>2</sup>Department of Endocrinology and Diabetes, Karolinska University Hospital, Stockholm, Sweden. <sup>3</sup>Department of Nosocomial Infection Control, China Medical University, Shenyang, China. <sup>4</sup>Dermatology and Venereology division, Department of Medicine Solna, Center for Molecular Medicine and Ming Wai Lau Centre for Reparative Medicine, Karolinska Institutet, Stockholm, Sweden. <sup>5</sup>Department of Infectious Disease, China Medical University, Shenyang, China. <sup>6</sup>Departments of Medicine, Microbiology and Immunology, Indiana University, Indianapolis, IN, USA. <sup>7</sup>Department of Anesthesia and Intensive Care Medicine, Aalborg University Hospital, Aalborg, Denmark. <sup>8</sup>Center for Diabetes, Academic Specialist Centrum, Stockholm, Sweden. <sup>9</sup>These authors contributed equally: Xiaowei Zheng, Sergiu-Bogdan Catrina. ✉email: [Xiaowei.zheng@ki.se](mailto:Xiaowei.zheng@ki.se); [Sergiu-Bogdan.Catrina@ki.se](mailto:Sergiu-Bogdan.Catrina@ki.se)

**W**ound healing is a complex process with high energy demands that involves several cellular compartments including keratinocytes, fibroblasts, endothelial and immune cells. The high energy needs are metabolically challenging since the wound environment is highly hypoxic due to reduced oxygen supply secondary to loss of vascularization. Wound healing is impaired in diabetes, and diabetic foot ulcer (DFU) represents a devastating complication of diabetes with drastic consequences for patients and society. The energy balance in diabetic wounds is even more difficult to achieve since hypoxia is more profound than in normoglycemic wounds<sup>1</sup> and the cellular reactions to hypoxia are impaired in diabetes<sup>2</sup> due to repressed hypoxia inducible factor-1 (HIF-1) signaling<sup>3</sup>. Local pharmacological reversal of the repressed HIF-1 signaling in diabetes is followed by the promotion of wound healing secondary to the improvement of several energy-demanding processes i.e. angiogenesis, dermal and epidermal regeneration<sup>1,4</sup>.

HIF-1 is a master regulator of oxygen homeostasis and therefore drives a large number of cellular processes. Currently, approximately 1000 human genes are identified to be directly influenced by HIF-1, which binds to the functionally cis-acting regulatory element called hypoxia response element (HRE)<sup>5</sup>.

MiR-210 is a unique microRNA that possesses an HRE and it is exclusively regulated in hypoxia by HIF-1 signaling<sup>6</sup> and it is modulated in a dose-dependent manner by oxygen<sup>7</sup>. miR-210 is ubiquitously expressed and influences the expression of a cluster of genes that are involved in processes highly relevant for energy metabolism and for tissue regeneration including angiogenesis, cell proliferation/apoptosis, and metabolic adaptation<sup>8</sup>. It has previously been shown that miR-210 has higher expression levels at the edge of ischemic wounds and inhibits keratinocyte proliferation<sup>9</sup>, and that anti-miR-210 treatment could accelerate healing of ischemic wounds<sup>10</sup>. However, to our knowledge, the regulation and function of miR-210 in diabetic wound has not been investigated before.

In this study, we investigated the contribution of miR-210 for the hypoxia signature in wound healing in diabetes. We show that the induction of miR-210 is repressed in the wounds of diabetic patients and in experimental wounds of diabetic db/db mice. Local reconstitution of miR-210 improved wound healing specifically in db/db mice by restoring metabolic balance and improving processes central to wound healing.

## Results

**High glucose levels inhibit the induction of miR-210 expression in hypoxia.** We first investigated the modulation of miR-210 expression by hypoxia in human dermal fibroblasts (HDF), human dermal microvascular endothelial cells (HDMEC), and keratinocytes, which are the most functionally relevant cellular components of the skin. As expected, hypoxia induced miR-210 expression in a time-dependent manner in all the three cell types (Fig. 1a–c). High glucose concentrations, however, diminished the hypoxia-induced expression of miR-210 in these cells (Fig. 1d–f).

**miR-210 expression is inhibited in diabetic wounds.** In response to the hypoxic environment, wound miR-210 expression was increased compared with that of skin in normoglycemic mice, as shown by both in situ hybridization (Fig. 2a) and quantitative RT-PCR analysis (Fig. 2b). The db/db mouse model is a widely validated model for investigating the impaired mechanisms of wound healing in diabetes<sup>11</sup>, in which the hypoxic environment was confirmed<sup>1</sup> exactly as in humans<sup>3</sup>. Although wounds of db/db diabetic mice are more hypoxic than those of normoglycemic mice<sup>1</sup>, miR-210 expression was significantly

lower in the wounds of db/db mice (Fig. 2a, b). These repressed levels of miR-210 reflect the impaired HIF-1 signaling in diabetic wounds<sup>1</sup> since they could be reversed when HIF-1 signaling was restored by local treatment with Dimethylxylglycine (DMOG) known to be able to overcome the repressing effect of diabetes on HIF-1 signaling<sup>2</sup> (Fig. 2e, f). Moreover, miR-210 expression was reduced in DFU compared to age-matched nondiabetic venous ulcer (VU) subjects (Fig. 2c, d). Taken together, these results suggest that reduced miR-210 expression may contribute to the impaired wound healing in diabetes.

**Local reconstitution of miR-210 in the wounds improves wound healing specifically in diabetes.** In order to examine the pathophysiological relevance of the impaired induction of miR-210 during wound healing in diabetes, we investigated the effects of locally injected miR-210 mimic, a stabilized form of miR-210, on wound healing rate of db/db mice. miR-210 reconstitution promoted wound healing in db/db mice (Fig. 3a–c) despite persistent profound hyperglycemia (Supplementary Fig. 1a, b). The positive effect of miR-210 on wound healing was driven locally since practically no systemic distribution was detected (Supplementary Fig. 1c). Interestingly, miR-210 improved the wound-healing rate specifically in diabetic mice, with no effect on the wound-healing rate in nondiabetic mice (Fig. 3d, e).

The histological examination of the wounds revealed that miR-210 improved several cellular processes essential for wound healing. The overall increase in the granulation tissue (Fig. 3f) followed an increase in the cellular proliferation rate as evaluated by ki67 (Fig. 3i) and angiogenesis as evaluated by CD31 immunostainings (Fig. 3h), which were characteristically impaired during wound healing in diabetes. miR-210 also increased collagen deposition in the granulation tissue of diabetic wounds as assessed by the Masson–Goldner Trichrome staining (Fig. 3g). The prolonged inflammatory phase characteristic of diabetic wounds, denoted by an elevation in the CD11b expression, was also normalized by miR-210 reconstitution (Fig. 3j).

**miR-210 restores metabolic balance in diabetic wounds.** Taking into account the aforementioned effects of miR-210 on cellular processes that require high energy and the known effect of miR-210 on the energy metabolism<sup>12</sup>, we decided to explore the role of miR-210 on the cellular metabolism during wound healing. Indeed, among the five validated potential mitochondrial target genes of miR-210<sup>13</sup>, local administration of miR-210 repressed the expression of two genes that are central for mitochondrial function, namely *Iron-sulfur cluster assembly enzyme (ISCU)* and *D-subunit of Succinate dehydrogenase (SDHD)* (Fig. 4a).

In agreement with its effects on these mitochondrial target genes, the administration of miR-210 had a profound influence on mitochondrial respiration by reversing the increased oxygen consumption rate (OCR) in db/db wounds to the levels found in the wounds from control nondiabetic mice (Fig. 4b). Interestingly, miR-210 reconstitution also led to an increase in the production of lactate (Fig. 4c), denoting an increase in glycolysis. Although this metabolic reprogramming did not result in a net increase in the ATP production (Supplementary Fig. 2), it contributed to reduced ROS levels in db/db wounds after local miR-210 mimic administration (Fig. 4d).

**Metabolic reprogramming by miR-210 improves fibroblast function.** Since the bulk of the granulation tissue consists of fibroblasts, it was of interest to study the effects of miR-210 in these cells in diabetic setting. In accordance with the findings in db/db wounds, miR-210 mimic transfection in HDFs exposed to

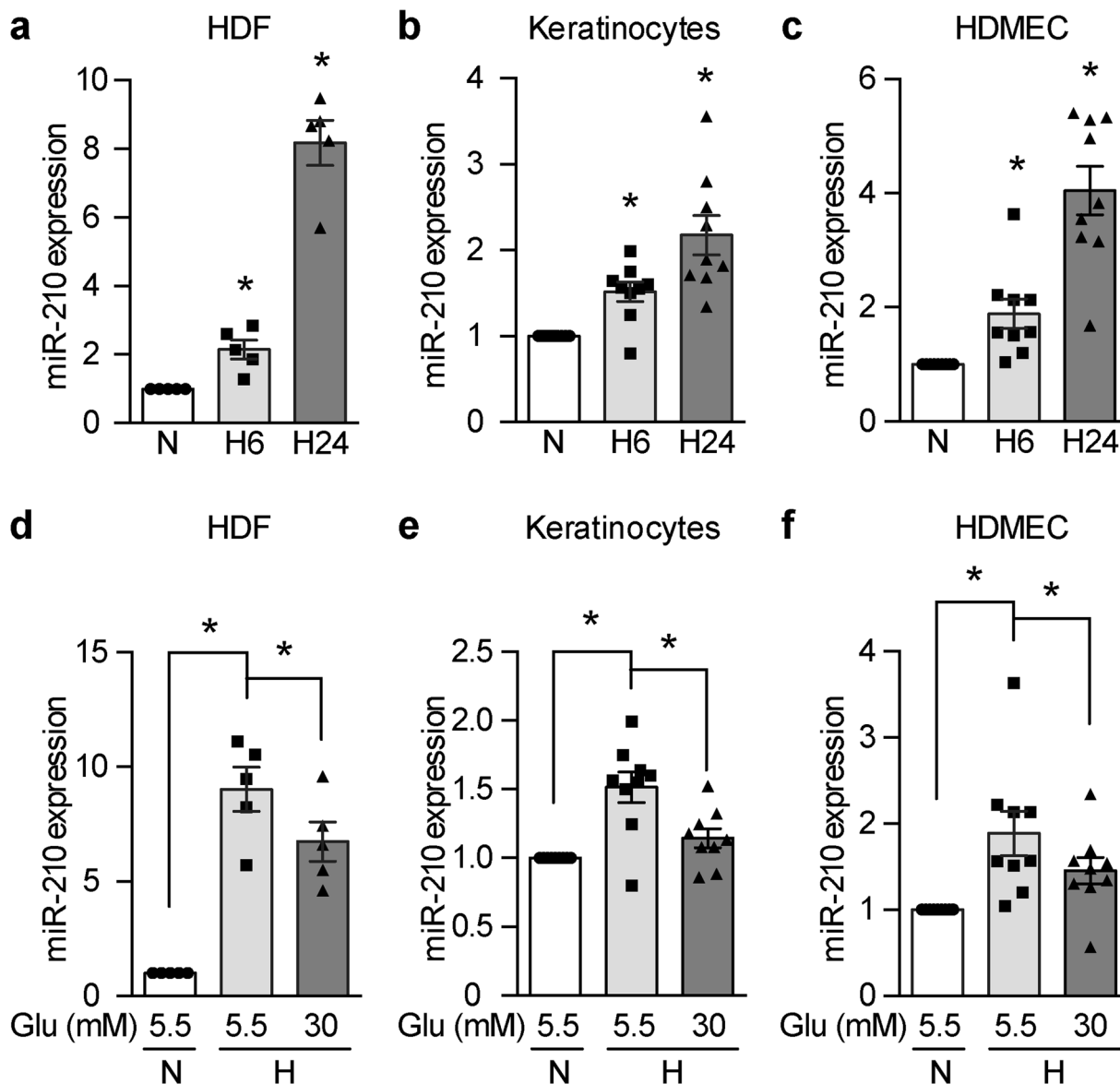


**Fig. 1 High glucose levels inhibit miR-210 induction at hypoxia.** **a–c** miR-210 expression in human dermal fibroblasts (HDF) ( $n = 5$ ), human dermal microvascular endothelial cells (HDMEC) ( $n = 9$ ), and keratinocytes ( $n = 9$ ) that were exposed to normoxia (N) or hypoxia for 6 h (H6) and 24 h (H24).  $*P < 0.05$  compared with N. **d–f** The cells were cultured in normal (5.5 mM) or high (30 mM) glucose (Glu) levels for 24 h and exposed to normoxia (N) or hypoxia (H) for 24 h (**d**) and 6 h (**e, f**) respectively. Relative miR-210 levels are shown. Statistical differences were calculated by one-way ANOVA. Data are represented as mean  $\pm$  s.e.m.  $*P < 0.05$ .

hypoxia and high glucose concentrations led to a significant decrease in the mRNA levels of *ISCU* and *SDHD* (Fig. 5a and Supplementary Fig. 3a). Moreover, miR-210 reconstitution decreased OCR (Fig. 5b), enhanced glycolysis (Fig. 5c) and diminished ROS levels (Fig. 5d) in HDFs exposed to hypoxia and high glucose levels. The metabolic changes induced by miR-210 reconstitution was further validated by the real-time ATP synthesis rate assay on a Seahorse XF analyzer. As shown in Fig. 5e, a significantly smaller proportion of ATP was generated via mitochondria respiration and a higher proportion of ATP was generated by glycolysis after miR-210 reconstitution in HDFs that were exposed to high glucose levels in hypoxia. We have further investigated the functional implications of the miR-210-induced metabolic reprogramming by evaluating the migration of HDF. The miR-210-induced migration of HDF exposed to high glucose levels in hypoxia was abrogated when glycolysis was inhibited in different ways by, namely, 2-deoxy-D-glucose (2-DG),

syrosingopine and sodium oxamate in HDFs (Fig. 5f and Supplementary Fig. 3b). This suggests that the positive effect of miR-210 on HDF migration is mediated by an increase in glycolysis. Taken together, these results indicate that miR-210 could reprogram the cellular energy metabolism which in turn improves the cellular function under diabetic conditions.

## Discussion

The high cellular energy demands during wound healing depends on an appropriate metabolic shift to cope with the low oxygen levels<sup>14</sup>. A pivotal role for the adequate reaction to hypoxia and for wound-healing processes is played by HIF-1 signaling that is responsible for the adaptation of metabolism, cellular motility and proliferation, immune response and angiogenesis<sup>15</sup>. DFU are however characterized by a repressed HIF-1 activation with direct negative consequences for wound healing<sup>3</sup>. Reactivation of HIF-1



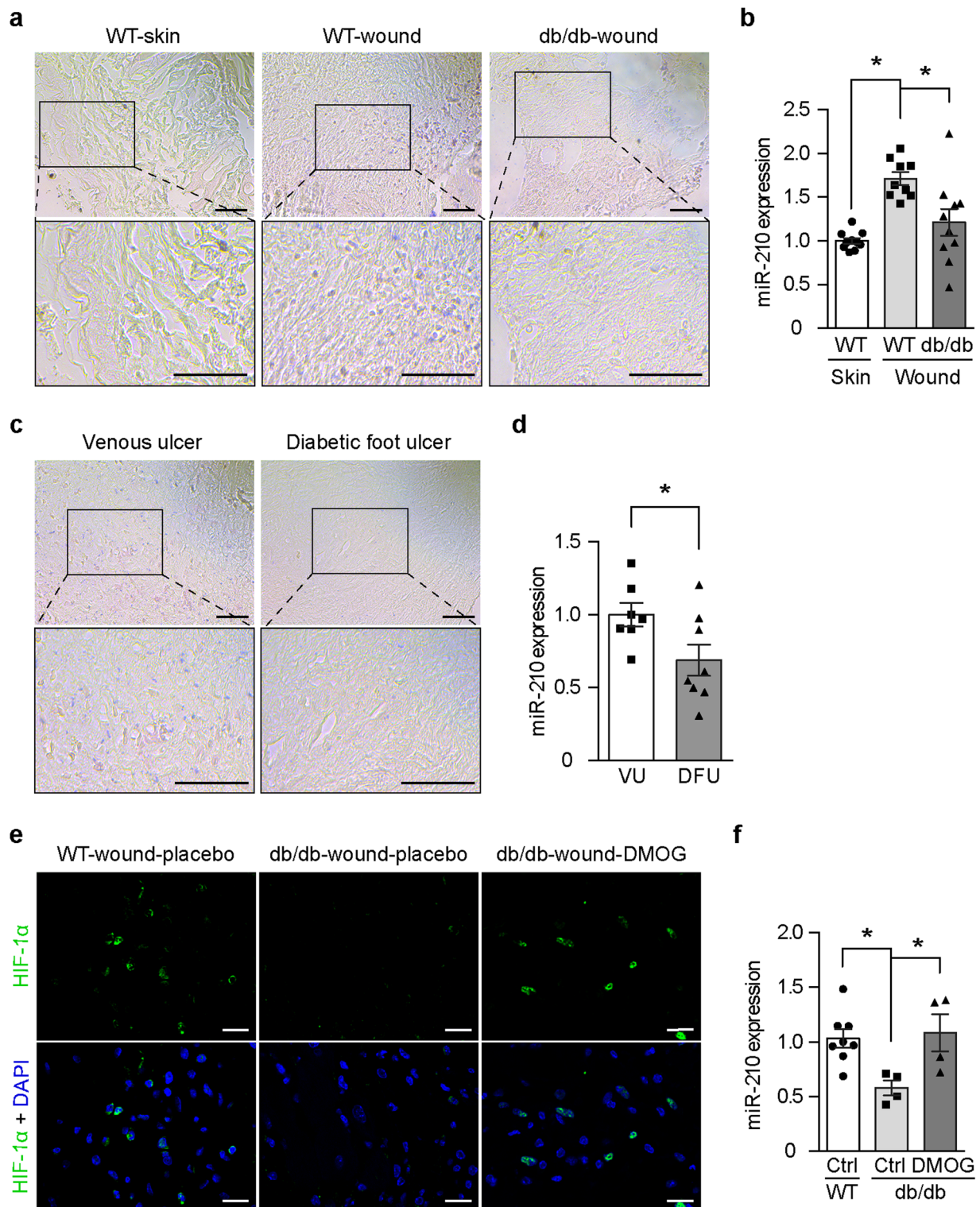


**Fig. 2** Reduced miR-210 expression in diabetic wounds. **a, b** miR-210 expression levels were analyzed in skin ( $n = 10$ ) and wounds ( $n = 9$ ) from normoglycemic wild-type (WT) mice, as well as in wounds from db/db diabetic mice ( $n = 10$ ) using in situ hybridization (**a**) and quantitative RT-PCR (**b**). **c, d** Wound biopsies from diabetic foot ulcers (DFU,  $n = 8$ ) and venous ulcers (VU,  $n = 7$ ) were analyzed for miR-210 expression using in situ hybridization (**c**) and quantitative RT-PCR (**d**). Scale bar = 50  $\mu\text{m}$ . HIF-1 $\alpha$  expression was analyzed by immunofluorescence (**e**) and miR-210 expression levels by quantitative RT-PCR (**f**) in wounds from WT-control mice ( $n = 8$ ) and wounds from db/db mice treated with placebo ( $n = 4$ ) or with DMOG ( $n = 4$ ). Scale bar = 100  $\mu\text{m}$ . Statistical differences were calculated using one-way ANOVA (**b, f**) and Student's *t* test (**d**). Data are represented as mean  $\pm$  s.e.m. \* $P < 0.05$ .

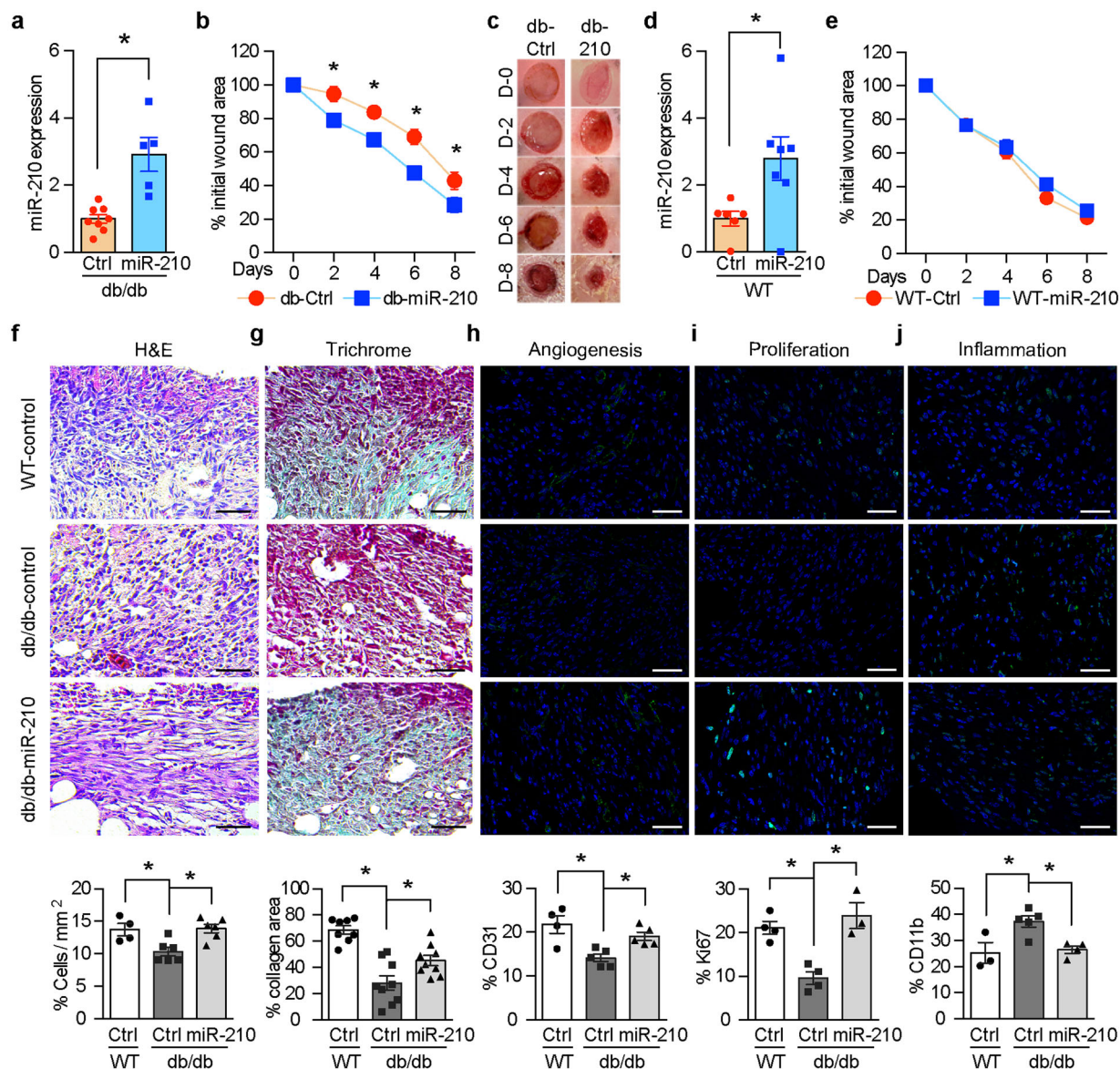


**Fig. 3 Local miR-210 administration improves wound healing specifically in diabetes.** Full-thickness excisional wounds were made on the dorsum of db/db and WT control mice, and control mimic (Ctrl) or miR-210 mimic (miR-210) was injected intradermally in the wound edge on day 0 and day 6. Wounds were harvested on day 8. **a, d** miR-210 expression in wounds analyzed by quantitative RT-PCR ( $n = 6, 7, 8, 5$  for WT-Ctrl, WT-miR-210, db/db-Ctrl and db/db-miR-210 groups, respectively). **b, e** Wound images were obtained every alternate days and wound healing rate is shown as the percentage of the initial wound area ( $n = 10, 11, 12, 14$  for WT-Ctrl, WT-miR-210, db/db-Ctrl and db/db-miR-210 groups, respectively). **c** Representative wound images during the healing process. **f–j** Levels of granulation, collagen deposition, proliferation, angiogenesis and inflammation were evaluated by histological analysis of H&E staining (**f**  $n = 4, 6$  and  $6$  for WT-Ctrl, db/db-Ctrl and db/db-miR-210 groups, respectively), Masson–Goldner Trichrome staining (**g**  $n = 8, 9$  and  $9$  for WT-Ctrl, db/db-Ctrl and db/db-miR-210 groups, respectively), CD31 (**h**  $n = 4, 5$  and  $5$  for WT-Ctrl, db/db-Ctrl and db/db-miR-210 groups, respectively), Ki67 (**i**  $n = 4, 4$  and  $3$  for WT-Ctrl, db/db-Ctrl and db/db-miR-210 groups, respectively), and CD11b staining (**j**  $n = 3, 5$  and  $4$  for WT-Ctrl, db/db-Ctrl and db/db-miR-210 groups, respectively). Results of semiquantitative evaluations are presented in the histograms. Statistical differences were calculated using Student's *t* test (**a, d**), two-way ANOVA (**b, e**) and one-way ANOVA (**f–j**), respectively. Data are represented as mean  $\pm$  s.e.m. \* $P < 0.05$ .

signaling in diabetic wounds is sufficient to reverse the wound-healing potential<sup>1</sup>. A clinical study that addresses the effects of activation of the HIF-1 signaling in DFU is ongoing (ClinicalTrials.gov Identifier: NCT03137966). The targets of HIF-1 signaling is however broad and modulate several cellular pathways that might not be involved in wound-healing process. It is therefore of value to explore a narrower relevant hypoxic signature for just the processes important for wound healing. Here we show that miR-210, which directly regulates approximately 30 genes<sup>13</sup>, is sufficient to improve the impaired wound healing specifically in diabetes.

The induction of miR-210 by hypoxia is in perfect agreement with its exclusive regulation by HIF-1 signaling and its ubiquitous expression<sup>6,7</sup>. The central regulatory role of HIF-1 for miR-210 function explains the repressive effect of hyperglycemia on miR-210 induction in hypoxia observed in cells and in vivo, which mirrors the well-documented glucose-dependent suppression of HIF-1 signaling in hypoxia<sup>16</sup>. Low expression of miR-210 has been reported in the pancreatic islets of diabetic animals and contributes to beta cell death<sup>17</sup>. On the other hand, high levels of miR-210 were reported in the serum and urine of patients with newly diagnosed Type 1 Diabetes<sup>18–20</sup>, and the hearts of



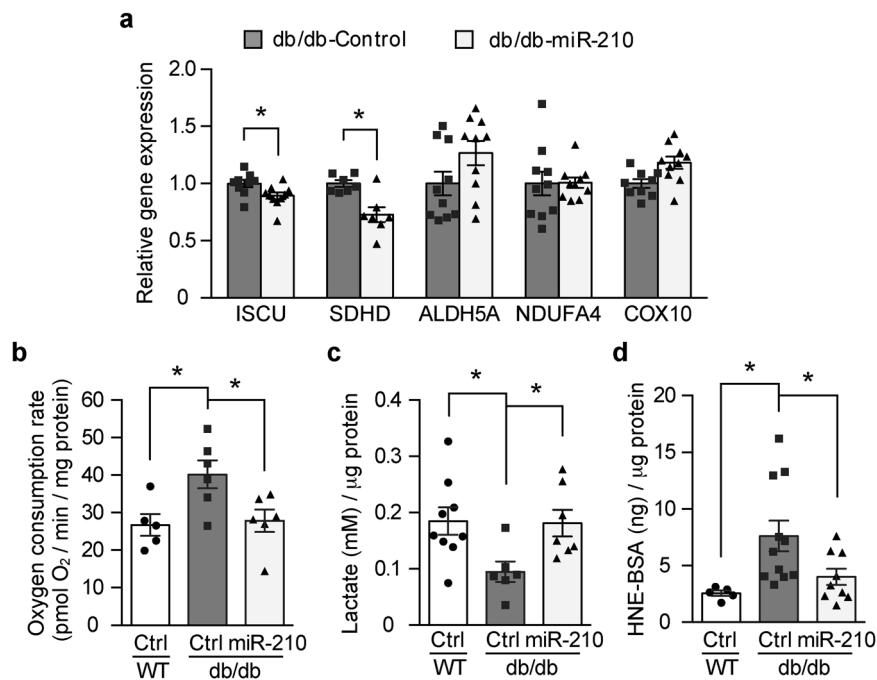


**Fig. 4 miR-210 restores metabolic balance in diabetic wounds.** **a** Gene expression of mitochondrial targets of miR-210—*ISCU*, *SDHD*, *ALDH5A*, *NDUFA4* and *COX10* were analyzed from control mimic or miR-210 mimic injected db/db wounds ( $n = 7-10$ ). **b** Oxygen consumption rate was analyzed from freshly harvested wounds using Seahorse XF Analyzer ( $n = 5, 6$  and  $6$  for WT-Ctrl, db/db-Ctrl and db/db-miR-210 groups, respectively). **c** Lactate levels were detected from tissue lysates ( $n = 9, 6$  and  $7$  for WT-Ctrl, db/db-Ctrl and db/db-miR-210 groups, respectively). **d** ROS levels were measured by detecting the amount of 4-HNE in the control mimic or miR-210 mimic injected wounds ( $n = 5, 11$  and  $9$  for WT-Ctrl, db/db-Ctrl and db/db-miR-210 groups, respectively). Statistical differences were calculated by one-way ANOVA. Data are represented as mean  $\pm$  s.e.m. \* $P < 0.05$ .

diabetic rats<sup>21</sup>, but the levels were not corrected for tissue oxygen tensions that are generally lower in diabetic tissues<sup>16,22</sup>. Similar to HIF-1 $\alpha$  expression, the miR-210 expression in diabetic tissues is dependent on the balance between the induction by hypoxia and the inhibition by high glucose levels. It is not surprising to detect higher miR-210 levels in diabetic tissues since they are more hypoxic than the corresponding controls which are not hypoxic. The inhibitory effects of high glucose concentrations will be unveiled when comparing hypoxic conditions with similar oxygen tensions or after correction for tissue oxygen concentrations. Our results showed that miR-210 expression increased in response to hypoxia in control wounds but was inhibited by hyperglycemia in diabetic wounds despite a more profound hypoxia<sup>1</sup>. This is confirmed by the fact that miR-210 increases to normal levels when impaired HIF-1 signaling in diabetes is rescued by the local treatment with DMOG. This confirms the insufficient adaptive response to hypoxia in diabetic wounds, which contributes to impaired wound healing.

The characteristically glucose-dependent impairment of cellular functions central for wound healing such as repressed proliferation, migration, and angiogenesis and increased inflammation were at least partially attributable to the decreased miR-210 expression in diabetic wound since its reconstitution restored them. miR-210 reconstitution improved granulation, proliferation and angiogenesis in the same way as the induction of HIF-1 signaling does in diabetic wounds<sup>1</sup>. The positive effect of miR-210 on angiogenesis is in agreement with previous reports showing miR-210 modulates endothelial cell response<sup>23</sup> and promotes angiogenesis in ischemic tissues<sup>24,25</sup>. The stimulatory effects of miR-210 on cell proliferation and migration are in line with previous observations in normal or transformed cells<sup>23,26-28</sup>. However, this effect seems to be dependent on cellular context and on oxygen levels<sup>9,29</sup>.

The reconstitution of miR-210 in the wounds of diabetic mice was sufficient to improve healing despite persistent hyperglycemia. It is highly specific for diabetic condition probably because of the disease-dependent inhibition of miR-210 during diabetic wound healing but it has no effect when it is expressed at sufficient levels during normal wound healing. Extremely high expression of miR-210 can even have a retarding effect on wound healing since it mimics profound ischemic conditions that are notorious for their deleterious effects on tissue regeneration<sup>9</sup>. It is interesting that inhibition of miR-210 was also followed by improvement in wound-healing rate in a model of impaired healing in diabetes<sup>30</sup>. The apparently opposing effects of miR-210 might be due to the differences in pharmacokinetics and wound models but might also mirror the fact that the biological effects of the hypoxamiR-210 are a mixture between its direct effects and the indirect effects played through HIF-1, which might be differently modulated by different pharmacological approaches.

The beneficial effects of miR-210 on the improvement of wound healing in diabetes can be at least partially explained by its effects on energy metabolism. The OCR of diabetic wounds was highly increased compared with nondiabetic wounds, which is in accordance with other reports on diabetic tissues<sup>31,32</sup>. Increased oxygen consumption results in hypoxia in diabetes in general<sup>22</sup>, and especially in diabetes wounds<sup>1</sup> due to the mismatch with oxygen delivery. It might well activate a vicious circle since the central mechanism for the adaptive responses to hypoxia, HIF-1 signaling, is repressed in diabetes<sup>16</sup>. Our data demonstrate that miR-210 diminished OCR in diabetic wounds as well as in HDFs exposed to high glucose concentrations in hypoxia. miR-210 could achieve this by downregulating *ISCU*, which is required for the formation of iron-sulfur cluster that is present in various enzymes of the tricarboxylic acid (TCA) cycle. miR-210 also reduced the expression levels of *SDHD*, an enzyme that takes part

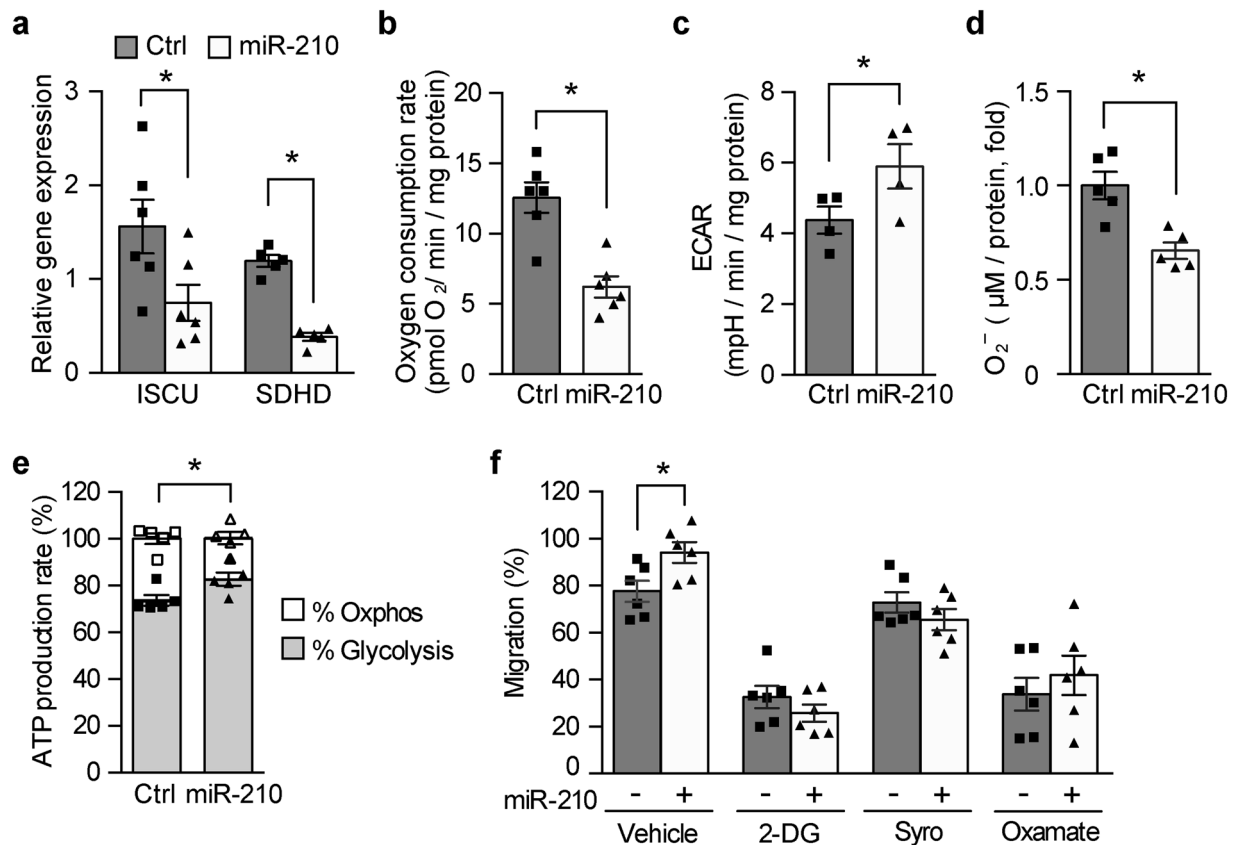


**Fig. 5 Metabolic reprogramming by miR-210 improves fibroblasts function.** HDF cells were transfected with control mimic or miR-210 mimic and exposed to hypoxia and high glucose concentration (30 mM) followed by measurement of **a** gene expression levels of *ISCU* ( $n = 6$ ) and *SDHD* ( $n = 5$ ), **b** oxygen consumption rate (OCR) ( $n = 6$ ), **c** extracellular acidification rate (ECAR) ( $n = 4$ ), **d** ROS levels ( $n = 5$ ) and **e** mitochondrial and glycolytic ATP production rate ( $n = 5$ ). **f** Migration of HDF that were treated with vehicle or glycolysis inhibitors 2-deoxy-D-Glucose (2-DG, 15 mM), Syrosingopine (Syro, 10 μM), and Oxamate (45 mM) along with hypoxia and high glucose concentrations ( $n = 6$ ). Statistical differences were calculated using paired Student's *t* test. Wilcoxon matched-pairs signed rank test was used for Syrosingopine-treated groups where the data were not normally distributed. Data are represented as mean  $\pm$  s.e.m. \* $P < 0.05$ .

in both TCA cycle and the electron transport chain (ETC) in the mitochondria. Moreover, miR-210 could enhance glycolysis that was inhibited in diabetic compared with nondiabetic control wounds. ROS levels were diminished by miR-210 as a consequence of the restoration of the balance between mitochondrial respiration and glycolysis. The enhanced glycolysis mediated the positive effects of miR-210 on the migration of HDF that were exposed to high glucose levels in hypoxia. This is in perfect agreement with the emerging role of glycolysis in promoting angiogenesis<sup>33</sup> and other cellular processes involved in tissue repair and regeneration<sup>34,35</sup>.

In conclusion, our results demonstrate a metabolic change in diabetic wounds characterized by increased OCR and ROS levels and decreased glycolysis due to inhibited miR-210 expression by hyperglycemia. miR-210 reconstitution can reverse the metabolic changes by inhibiting OCR and enhancing glycolysis and consequently normalize ROS levels and promote wound healing specifically in diabetes (Fig. 6). These data suggest that local miR-210 administration in diabetic wounds is a promising therapeutic approach for DFU.

## Methods

**Chemicals.** Custom-stabilized miRIDIAN mmu-microRNA-210-3p mimic (C-310570-5) and custom-stabilized miRIDIAN negative control mimic #1 (CN-001000-01) were obtained from Dharmacon. MaxSuppressor™ In Vivo RNA-LANCER II was from BIOO Scientific, RNAlater™ Stabilization solution were obtained from ThermoFisher Scientific, 10% neutral buffered formalin solution from Sigma, and Mayers Hemotoxylin and 0.2% Eosin from Histolab. Mmu-miR-

210-3p-specific LNA-probes were obtained from Exiqon. 2-deoxy-D-Glucose, Syrosingopine and sodium oxamate were purchased from Sigma Aldrich.

**Human wound biopsies.** Eight patients with DFU (age:  $69.1 \pm 9.9$  years old; HbA1c:  $59.71 \pm 11.52$  mmol/mol) and seven patients with venous ulcer (age:  $78.4 \pm 6.9$  years old) were recruited after agreeing and providing their informed consent. Detailed information of these subjects is given in Table 1. The Regional Ethical Review Board in Stockholm, Sweden approved the study. The wound biopsies were taken using 4 mm biopsy punch after local anesthesia.

**Animals.** BKS(D)-*Lepr<sup>db</sup>/J*OrIRj (db/db) mice and their corresponding normoglycemic wild-type (WT) control mice were obtained from Janvier Labs. The mice were housed up to five per cage in a 12-h light/dark cycle at 22 °C and were provided standard laboratory food and water ad libitum. The animals were caged individually and handled daily for 1 week before wounding. The mice were randomized into groups receiving control microRNA mimic or miR-210 mimic according to their HbA1c levels, body weight and blood glucose levels. The sample size was determined using power calculations based on the results from the same mouse model in our previous studies<sup>1,36</sup>.

**Wound model.** The wound model was created as described previously<sup>1</sup>. Following blood glucose control, the mice were anesthetized and the hair from the back were removed using a shaver followed by a depilatory cream. The skin was cleaned with 70% ethanol and two full-thickness wounds extending through the panniculus carnosus were created on either side of the dorsal midline using a 6-mm biopsy punch. MiR-210 mimic (0.125 nmol) or negative control mimic were injected intradermally at four different places in the wound edges on the day of wounding as well as after 6 days post surgery. In wound experiment using DMOG, 100 μL DMOG (2 mM) or vehicle were applied locally every other day. Digital photographs were obtained on the day of wounding and every other day after wounding. A circular reference of known area was placed alongside the wounds to allow for correction of the distance between the camera and the wound. The wound area was



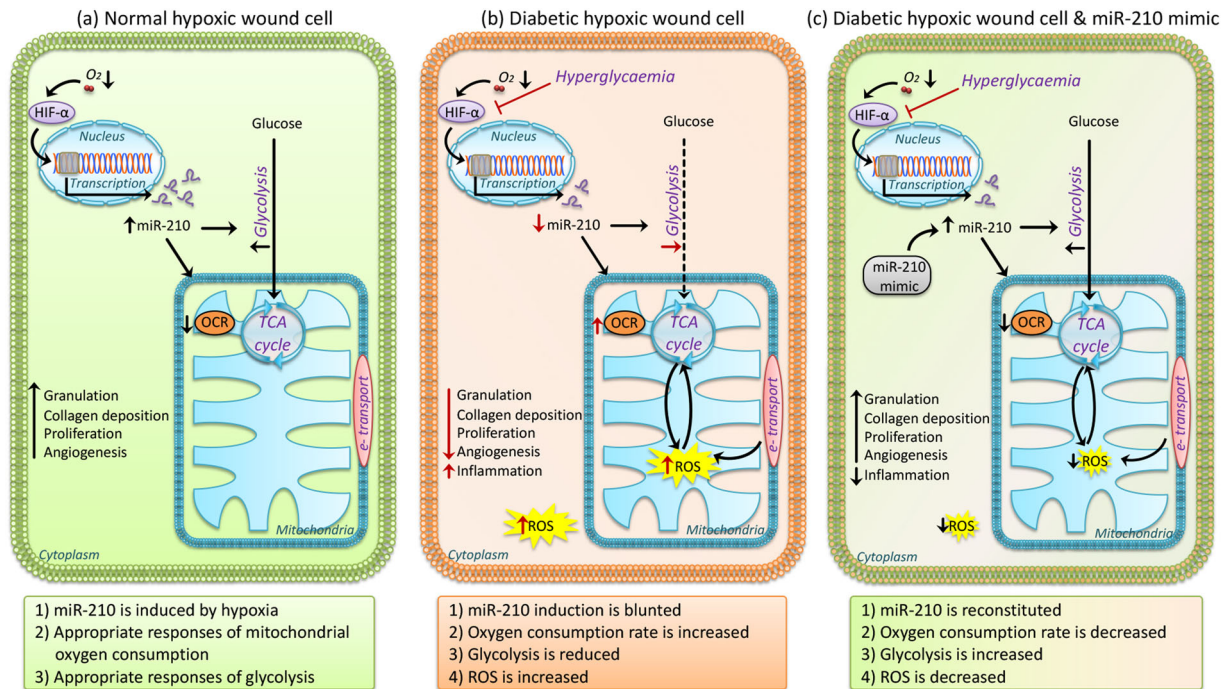


**Fig. 6 Schematic illustration of the cellular metabolic changes in diabetic wounds that can be reversed by miR-210 reconstitution.** **a** In normal hypoxic wound cell, miR-210 is induced by hypoxia and regulates appropriate responses of mitochondrial oxygen consumption (OCR) and glycolysis. **b** In diabetic hypoxic wound cell, miR-210 induction is blunted, resulting in increased OCR, reduced glycolysis, and consequently elevated ROS levels which are detrimental to wound healing. **c** In miR-210-reconstituted diabetic hypoxic wound cells, miR-210 can reverse the metabolic changes by inhibiting OCR and enhancing glycolysis and consequently normalize ROS levels which are beneficial for wound healing.

calculated using ImageJ software, version 1.47 (NIH, USA), corrected for the area of the reference circle and expressed as percentage of the original area. The data analysis was blinded. On day 8 after wounding, the animals were euthanized and the wounds were harvested. One part of the wounds was snap frozen, one part was placed in RNALater and the rest used for Seahorse analysis. One half of the other wound was placed in 10% formalin to be processed for histology and staining.

**Histology.** Histology was performed on formalin-fixed, paraffin-embedded sections (5  $\mu$ m). The slides were stained with hematoxylin and eosin after deparaffinization and rehydration. Subsequently, the granulation area of the wound was quantified. Image analysis and quantification was done using smart segmentation feature on Image Pro Premier software, version 9.2 (Media Cybernetics). At least two images from each slide were evaluated and each condition had 4–6 slides. Granulation was measured as ratio of the number of cells to the total area of the granulation layer in an image.

**Fluorescent immunohistochemistry.** Formalin-fixed, paraffin-embedded tissues (FFPE) were deparaffinized and rehydrated. Antigen retrieval was performed in a microwave (800 W for 10 min) using citrate buffer. Slides were then washed with PBS-T (Phosphate buffered saline supplemented with 0.1% Tween) 3 times for 3 min each. The sections were blocked with goat serum or 5% bovine serum albumin (BSA) in PBS for 30 min at RT, then incubated with primary antibodies overnight at 4 °C. After three times wash with PBS-T for 3 min each, the sections were incubated with fluorochrome-conjugated secondary antibody for 1 h at RT in dark. The sections were washed in PBS-T three times for 3 min each and treated with 0.1% Sudan Black-B solution (Sigma) for 10 min to quench autofluorescence. After washing, the sections were incubated with 1:5000 diluted DAPI (4',6-diamidino-2-phenylindole, Thermo-Fisher Scientific) in PBS for 5 min and followed by washing in PBS-T for 5 min. The sections were then mounted and stored in 4 °C. The fluorescent images were acquired using Leica TCS SP5 or SP8 confocal microscope (Leica Microsystems).

To detect HIF-1 $\alpha$ , the fluorescent signal was enhanced using Tyramide Superboost kit (ThermoFisher). Briefly, following antigen retrieval, the sections were blocked with 3% H<sub>2</sub>O<sub>2</sub> before blocking with goat serum. The sections were incubated with primary antibody and washed with PBS-T 5 min four times followed by incubation with an HRP-conjugated rabbit antibody for 1 h at RT. The sections were washed thoroughly and incubated with tyramide reagent for 10 min at RT in dark. The reaction was stopped by incubating with the stop solution for 5 min and three times washed with PBS-T for 3 min each. The sections were subsequently treated with 0.1% Sudan Black-B solution, followed by

counterstaining with DAPI (1:5000) for 5 min. The sections were finally washed with PBS-T and mounted.

Image analysis was performed using Image-Pro Premier, version 9.2 (Media Cybernetics) and ImageJ software, version 1.47 (NIH, USA). For CD31, Ki67 and CD11b staining, 2–5 images per tissue and a total of at least three tissues per condition were considered for image analysis. The total number of nuclei and cells with positive signal were counted. Quantification for each staining is expressed as percentage of positive cells to total number of cells. The following primary antibodies were used: anti-CD31 from Dianova (DIA310, 1:100); anti-Ki67 from Abcam (ab15580, 1:1000), anti-CD11b from Merck Millipore (MABF512, 1:100) and anti-HIF-1 $\alpha$  (GTX127309, 1:100). The secondary antibodies used were goat anti-rat Alexa Fluor 488 (A11006, 1:500) and goat anti-rabbit Alexa Fluor 488 (A11008, 1:500) from ThermoFisher Scientific.

**In situ hybridization.** For the detection of miR-210 in FFPE sections, Exiqon miRCURY locked nucleic acid (LNA)-DIG labeled probe was used as previously described<sup>37</sup> with some modifications. Briefly, FFPE slides (5  $\mu$ m thickness) were deparaffinized and the RNAs were demasked by 15  $\mu$ g/mL proteinase K treatment for 10 min at 37 °C. The probes were hybridized with Mmu-miR-210-3p-specific LNA-probes (Exiqon) at a concentration of 250 nM for 2 h at 53 °C. Stringent washes were carried out at 53 °C with decreasing concentrations of Saline-Sodium Citrate buffer (SSC) (once in 5 $\times$  SSC, twice in 1 $\times$  SSC and twice in 0.2 $\times$  SSC) for 5 min followed by a final wash with 0.2 $\times$  SSC at room temperature. The sections were then blocked and incubated with an alkaline phosphatase (AP)-conjugated antibody specific to DIG (Roche, 1:1000) for 1 h at room temperature. The signal for miR-210 was visualized by addition of an AP substrate, NBT/BCIP (ThermoFisher) and the slides were counterstained with nuclear fast red stain (Vectorlabs).

**Masson–Goldner Trichrome staining.** FFPE sections of wounds were deparaffinized with two passes in Xylene for 3 min each and rehydrated in sequential passes of 100% and 95% ethanol for 3 min, two times each. The slides were treated according to the manufacturer's instructions to obtain Masson–Goldner Trichrome staining (Merck Millipore). Images of the staining were obtained using Leica DM3000 LED fluorescence microscope using the transmitted light. The collagen stained areas in the wounds were analyzed and quantified using the Smart Segmentation feature on Image Pro Premier software, version 9.2 (Media Cybernetics). At least 2–4 images from 3 to 4 tissues from each condition were analyzed. Collagen staining was expressed as the percentage of area stained by collagen (green).

**Table 1 Information of patients with diabetes and controls.**

| Donor | Group | Gender | Age | HbA1c (mmol/mol) | Diagnosis  | Medication   |
|-------|-------|--------|-----|------------------|--|--|
| 01    | DFU   | M      | 66  | 45               | T2DM, DFU, hypertension, renal failure stage 3, TIA                                | Metformin, Insulin Aspart, Insulin Glargine, Atenolol, Lisinopril, Fluoxacillin  |
| 02    | DFU   | F      | 57  | 63               | T2DM, DFU, osteomyelitis, chronic charcot foot                                     | Fluoxacillin, Sitagliptine, Repaglinide, Furosemide, Felodipine, Enalapril, Atorvastatin, Oxycodone  |
| 03    | DFU   | M      | 60  | 74               | T2DM, DFU, hypertension  | Metformin, Insulin Aspart, Insulin Glargine, Atenolol, Lisinopril, Fluoxacillin  |
| 04    | DFU   | M      | 81  | 45               | T2DM, DFU, dyslipidemia, TIA, CAD, CML   | Insulin Aspart, Insulin Protamine, Acetylsalicylic acid, Imatinib, Bisoprolol, Furosemide, Fluoxacillin  |
| 05    | DFU   | M      | 70  | 51               | T2DM, DFU, renal failure stage 3   | Insulin Glargine   |
| 06    | DFU   | M      | 69  | —                | T2DM, DFU, hypertension, dyslipidemia  | Insulin Glargine, Metformin  |
| 07    | DFU   | M      | 86  | 61               | T2DM, DFU, hypertension, dyslipidemia, atrial fibrillation, TIA, CHF, Charcot foot | Insulin Aspart, Insulin Protamine  |
| 08    | DFU   | M      | 64  | 79               | T2DM, DFU, hypertension, dyslipidemia, renal failure stage 3, COPD                 | Insulin Glargine, Insulin Aspart, Acetylsalicylic acid, Furosemide, Metoprolol, Enalapril, Simvastatin, Ciprofloxacin  |
| VU1   | VU    | M      | 86  | —                | VU, prostate cancer, depression, cardiac insufficiency, polycythemia vera          | Omeprazole, calcium carbonate, and cholecalciferol, Furix, Metoprolol, Losartan, Oxycodone, Paracetamol, Zopiclone, Mirtazapine, Warfarin, Prednisolone, Lactulose, Enantion Depot |
| VU2   | VU    | F      | 78  | —                | VU, atherosclerosis in extremity arteries  | Tromblyl, Simvastatin, Oxycodone, Clopidrogel  |
| VU3   | VU    | F      | 71  | —                | VU, atrial fibrillation, venous thrombosis   | Calcium carbonate, Potassium chloride, Fragmin, Iron sulfate, Bisoprolol   |
| VU4   | VU    | F      | 77  | —                | VU, skin defect after surgery  | Prednisolon, Paracetamol, Tramadol, Calcium carbonate, losartan, Etarnecept  |
| VU5   | VU    | F      | 87  | —                | VU, varices, peripheral atherosclerosis  | Sodium chloride, Paracetamol   |
| VU6   | VU    | M      | 69  | —                |  | Split skin graft   |
| VU7   | VU    | F      | 81  | —                |  |  |

T2DM type 2 diabetes, DFU diabetes foot ulcer, VU venous ulcer, TIA transient ischemic attack, CVD cardiovascular disease, COPD chronic obstructive pulmonary disease.

**4-Hydroxynonenal measurement.** 4-Hydroxynonenal (4-HNE) was measured in frozen wound lysates using commercially available kits (OxiSelect STA-838 and STA-310, Cell Biolabs, San Diego, CA, USA) according to the manufacturer's instructions.

**Lactate assay.** Lactate production was measured using the Lactate Colorimetric Assay kit from Biovision according to the manufacturer's instructions. Wound tissues were homogenized in lactate assay buffer provided in the kit and lactate levels were measured and normalized to the protein levels.

**Cell culture.** Primary HDFs (ATCC, USA) were cultured in Dulbecco's modified Eagle's medium (DMEM; 5.5 mM glucose) supplemented with 100 IU/ml penicillin and streptomycin, and 10% heat-inactivated FBS (fetal bovine serum, Invitrogen). The cells were maintained in a humidified atmosphere with 5% CO<sub>2</sub> at 37 °C in a cell culture incubator, and passages 4–9 were used for experiments. Cells were cultured under normoxic [21% O<sub>2</sub> (vol/vol)] or hypoxic (1% O<sub>2</sub>) conditions in Hypoxia Workstation INVIVO2 (MedicalExpo).

**Transfection of miR-210 mimic in HDF.** HDFs were transfected with miR-210 mimic or negative control mimic using Lipofectamine RNAiMAX (Life Technologies) according to the manufacturer's instructions. The cells were harvested 24–48 h after transfection. Total RNA was extracted and the expression levels of miR-210 were analyzed.

**RNA purification and quantitative RT-PCR.** Total RNA, including microRNAs, was extracted from cells and tissues using a miRNeasy RNA extraction kit (Qiagen). To detect mRNA expression, high-capacity cDNA Reverse Transcription Kit (ThermoFisher Scientific) was used. All quantitative RT-PCR was performed on a 7300 Real-Time PCR System or QuantStudio 6 and 7 Flex Real-Time PCR System (Applied Biosystems) using SYBR Green Master Mix or Taqman Gene Expression Assays (ThermoFisher Scientific). The internal controls for mRNA expression were *PBGD* and *Actin*. The primer sequences for SYBR Green quantitative RT-PCR were: mouse *ALDH5A1\_F*: CCAGTCATCAAGTTTGATAAGGAG; mouse *ALDH5A1\_R*: GAGCCCTTCATTCACACC; mouse *NDUFA4\_F*: GCATCCCG CTTGATTCCT; mouse *NDUFA4\_R*: GTTTGCTGTAGTCCACATTCAC; mouse *ACTB\_F*: AAGATCAAGATCATTGCTCCTC; mouse *ACTB\_R*: GGACTCA TCGTACTCCTG; mouse *PBGD\_F*: TCCTGTTCAGCAAGAAGA; mouse *PBGD\_R*: GGCAGTGATTCACACCAG. TaqMan Gene Expression Assays were Mm02342800\_g1 for mouse *ISCU*; Mm00546511\_m1 for mouse *SDHD*; Mm00617695\_m1 for mouse *COX10*; Mm01143545\_m1 for mouse *PBGD*; and Mm02619580\_g1 for mouse  $\beta$ -actin.

**MicroRNA detection.** TaqMan microRNA Reverse Transcription kit and TaqMan miRNA assays (ThermoFisher Scientific) were used for the analysis of miR-210, U6 snRNA and snoRNA55 expression (assay IDs were 000512, 001228, and 001973 respectively). U6 was used as internal control for HDF and keratinocytes, and snoRNA55 was used as control for mouse tissues. To detect miR-210 expression in

HDFEC and human wounds, cDNA was produced using TaqMan Advanced miRNA cDNA Synthesis Kit (ThermoFisher Scientific) and microRNA expression was detected using TaqMan Advanced miRNA assays (ThermoFisher Scientific), where miR-103a or the average of miR-16, miR-23a, and miR-24 were used as internal controls. The TaqMan Advanced miRNA assays were hsa-miR-210-3p (477970\_mir), hsa-miR-103a-3p (478253\_mir), hsa-miR-16-5p (477860\_mir), hsa-miR-23a-3p (478532\_mir), and hsa-miR-24-3p (477992\_mir).

**In vitro migration assay.** HDF migration was studied using the scratch assay. Cells were plated in 24-well plates coated with collagen (50  $\mu$ g/ $\mu$ L) overnight and blocked with 3% BSA in PBS for 2 h. At 90% confluency, the cells were transfected with the miR-210 mimic or negative control mimic as mentioned above. At 24 h after transfection, a scratch was generated in each well with a micropipette tip. The cells were rinsed and treated with normal (5.5 mM) or high glucose (30 mM) medium supplemented with 0.2% FBS and the plates were placed in normoxia or hypoxia. Mitomycin C (10  $\mu$ g/mL) (Roche) was included in the media to prevent cell proliferation. Digital pictures were obtained immediately after scratching and after 16 h using EVOS XL Core Cell Imaging System (ThermoFisher Scientific). Images were analyzed using ImageJ, version 1.47 software (NIH, Bethesda, MD, USA). The experiment was done in triplicates and three images from each replicate were used for analysis. On each image, the distance between the two sides of the scratch was measured at certain intervals using ImageJ and the mean of distance was calculated. Migration rate was calculated as the difference between the mean of distance at 0 h (Distance\_0h) and 16 h (Distance\_16h) divided by the distance at 0 h ((Distance\_0h – Distance\_16h)/Distance\_0h). The migration rate for each condition was expressed as percentage to the control condition and was expressed as Relative Migration.

**Measurement of oxygen consumption, extracellular acidification, and ATP production rates.** Basal OCR, extracellular acidification rate (ECAR), and ATP production rate were measured using XF Cell Mito Stress Test kit, XF Glycolytic Rate Assay kit, and XF Real-Time ATP Rate Assay kit on Seahorse XF Analyzer (Agilent Technologies). The sensor cartridges used for measuring the oxygen flux was equilibrated in an XF Calibrant (Agilent Technologies) for 16–24 h before the experiment in a 0%-CO<sub>2</sub> 37 °C incubator. The granulation tissue from the wounds taken from mice after 8 days of wounding was carefully dissected and rinsed with unbuffered Krebs-Henseleit buffer (KHB) media. The tissue was placed at the bottom of the XF24 Islet Capture Microplate (Agilent technologies) and covered with a mesh. Four hundred and fifty microliters KHB medium was added to each well containing the tissue and equilibrated in a 0%-CO<sub>2</sub> incubator for 30 min. The cartridge was then placed on the assay plate and run in the XF analyzer using an optimized protocol to measure basal OCR. For analysis in cells, HDFs were transfected with negative control mimic or miR-210 mimic and treated with normal (5.5 mM) or high (30 mM) glucose levels in normoxia or hypoxia. The cells from each condition were then seeded onto an XF24 or XFe96 Cell Culture Microplate and (Agilent Technologies). The results were normalized to protein concentration or cell number as indicated.

**Electron paramagnetic resonance (EPR) spectroscopy.** ROS levels were measured using cyclohexyldiamine (CMH) spin probe and a CP radical standard curve, using EPR spectrometer (Noxygen, Elzach, Germany). HDF cells were transfected with miR-210 mimic/control mimic and were treated with normal or high glucose and hypoxia or normoxia 16 h after transfection. Following 24 h of treatment, media was removed and the cells were washed twice with PBS. Seven hundred microliters CMH buffer (200  $\mu$ M) was added to the cells and were incubated in a cell incubator for 30 min. The cells were collected in CMH buffer and were frozen in liquid nitrogen prior to measurement.

**Statistics and reproducibility.** Statistical analysis and graphing were performed using GraphPad Prism software (version 6). Outliers were identified using Grubbs' test. Normality of distribution was analyzed using the Kolmogorov-Smirnov test. Differences between two groups were analyzed using two-sided Student's *t* test for data with normal distribution, and nonparametric test was used for data that was not normally distributed. Multiple comparisons of three or more groups were performed using one-way ANOVA or two-way ANOVA followed by Bonferroni's post hoc test.  $P < 0.05$  was considered statistically significant. All measures were taken from distinct samples, and the sample sizes are presented in figure legends. All the in vitro experiments were performed at least three times independently. Data are presented as mean  $\pm$  standard error of the mean (s.e.m.).

**Study approval.** The experimental animal procedure was approved by the North Stockholm Ethical Committee for the Care and Use of Laboratory Animals. The study using human material was reviewed and approved by the Regional Ethical Committee of Stockholm. Written informed consent was received from participants prior to inclusion in the study. The study was conducted according to the Declaration of Helsinki's principles.

### Data availability

The datasets generated during and/or analyzed during the current study are available from the corresponding authors on reasonable request.

Received: 6 March 2020; Accepted: 15 November 2020;

Published online: 14 December 2020

### References

- Botusan, I. R. et al. Stabilization of HIF-1 $\alpha$  is critical to improve wound healing in diabetic mice. *Proc. Natl Acad. Sci. USA* **105**, 19426–19431 (2008).
- Catrina, S. B. & Zheng, X. Disturbed hypoxic responses as a pathogenic mechanism of diabetic foot ulcers. *Diabetes Metab. Res. Rev.* **32**, 179–185 (2016).
- Catrina, S. B., Okamoto, K., Pereira, T., Brismar, K. & Poellinger, L. Hyperglycemia regulates hypoxia-inducible factor-1 $\alpha$  protein stability and function. *Diabetes* **53**, 3226–3232 (2004).
- Thangarajah, H. et al. The molecular basis for impaired hypoxia-induced VEGF expression in diabetic tissues. *Proc. Natl Acad. Sci. USA* **106**, 13505–13510 (2009).
- Semenza, G. L. Hypoxia-inducible factor 1 and cardiovascular disease. *Annu. Rev. Physiol.* **76**, 39–56 (2014).
- Kulshreshtha, R. et al. A microRNA signature of hypoxia. *Mol. Cell Biol.* **27**, 1859–1867 (2007).
- Chan, S. Y. et al. MicroRNA-210 controls mitochondrial metabolism during hypoxia by repressing the iron-sulfur cluster assembly proteins ISCU1/2. *Cell Metab.* **10**, 273–284 (2009).
- Ivan, M., Harris, A. L., Martelli, F. & Kulshreshtha, R. Hypoxia response and microRNAs: no longer two separate worlds. *J. Cell Mol. Med.* **12**, 1426–1431 (2008).
- Biswas, S. et al. Hypoxia inducible microRNA 210 attenuates keratinocyte proliferation and impairs closure in a murine model of ischemic wounds. *Proc. Natl Acad. Sci. USA* **107**, 6976–6981 (2010).
- Ghatak, S. et al. AntihypoxamiR functionalized gramicidin lipid nanoparticles rescue against ischemic memory improving cutaneous wound healing. *Nanomed.: Nanotechnol., Biol., Med.* **12**, 1827–1831 (2016).
- Michaels, J. et al. db/db mice exhibit severe wound-healing impairments compared with other murine diabetic strains in a silicone-splinted excisional wound model. *Wound Repair Regen.* **15**, 665–670 (2007).
- Ivan, M. & Huang, X. miR-210: fine-tuning the hypoxic response. *Adv. Exp. Med. Biol.* **772**, 205–227 (2014).
- Bertero, T., Rezzonico, R., Pottier, N. & Mari, B. Impact of microRNAs in the cellular response to hypoxia. *Int. Rev. Cell Mol. Biol.* **333**, 91–158 (2017).
- Ninikoski, J., Heughan, C. & Hunt, T. K. Oxygen tensions in human wounds. *J. Surg. Res.* **12**, 77–82 (1972).
- Ruthenborg, R. J., Ban, J. J., Wazir, A., Takeda, N. & Kim, J. W. Regulation of wound healing and fibrosis by hypoxia and hypoxia-inducible factor-1. *Mol. Cells* **37**, 637–643 (2014).
- Catrina, S. B. Impaired hypoxia-inducible factor (HIF) regulation by hyperglycemia. *J. Mol. Med.* **92**, 1025–1034 (2014).
- Nesca, V. et al. Identification of particular groups of microRNAs that positively or negatively impact on beta cell function in obese models of type 2 diabetes. *Diabetologia* **56**, 2203–2212 (2013).
- Osipova, J. et al. Diabetes-associated microRNAs in pediatric patients with type 1 diabetes mellitus: a cross-sectional cohort study. *J. Clin. Endocrinol. Metab.* **99**, E1661–E1665 (2014).
- Assmann, T. S. et al. MicroRNA expression profile in plasma from type 1 diabetic patients: case-control study and bioinformatic analysis. *Diabetes Res. Clin. Pr.* **141**, 35–46 (2018).
- Nielsen, L. B. et al. Circulating levels of microRNA from children with newly diagnosed type 1 diabetes and healthy controls: evidence that miR-25 associates to residual beta-cell function and glycaemic control during disease progression. *Exp. Diabetes Res.* **2012**, 896362 (2012).
- Costantino, S., Paneni, F., Luscher, T. F. & Cosentino, F. MicroRNA profiling unveils hyperglycaemic memory in the diabetic heart. *Eur. Heart J.* **37**, 572–576 (2016).
- Bianchi, L. et al. Integrated cardiovascular/respiratory control in type 1 diabetes evidences functional imbalance: possible role of hypoxia. *Int. J. Cardiol.* **244**, 254–259 (2017).
- Fasanaro, P. et al. MicroRNA-210 modulates endothelial cell response to hypoxia and inhibits the receptor tyrosine kinase ligand Ephrin-A3. *J. Biol. Chem.* **283**, 15878–15883 (2008).
- Liu, F. et al. Upregulation of microRNA-210 regulates renal angiogenesis mediated by activation of VEGF signaling pathway under ischemia/perfusion injury in vivo and in vitro. *Kidney Blood Press. Res.* **35**, 182–191 (2012).
- Zaccagnini, G. et al. Hypoxia-induced miR-210 modulates tissue response to acute peripheral ischemia. *Antioxid. Redox Signal.* **21**, 1177–1188 (2014).
- Zhang, Z. et al. MicroRNA miR-210 modulates cellular response to hypoxia through the MYC antagonist MNT. *Cell Cycle* **8**, 2756–2768 (2009).
- Zhang, S., Lai, N., Liao, K., Sun, J. & Lin, Y. MicroRNA-210 regulates cell proliferation and apoptosis by targeting regulator of differentiation 1 in glioblastoma cells. *Folia Neuropathol.* **53**, 236–244 (2015).
- Li, Z. et al. Overexpression of microRNA-210 promotes chondrocyte proliferation and extracellular matrix deposition by targeting HIF-3 $\alpha$  in osteoarthritis. *Mol. Med. Rep.* **13**, 2769–2776 (2016).
- Bodempudi, V. et al. miR-210 promotes IPF fibroblast proliferation in response to hypoxia. *Am. J. Physiol. Lung Cell Mol. Physiol.* **307**, L283–L294 (2014).
- Dallas, A. et al. Acceleration of diabetic wound healing with PHD2- and miR-210-targeting oligonucleotides. *Tissue Eng. Part A* **25**, 44–54 (2019).
- Hartman, M. L. et al. Relation of mitochondrial oxygen consumption in peripheral blood mononuclear cells to vascular function in type 2 diabetes mellitus. *Vasc. Med.* **19**, 67–74 (2014).
- Persson, M. F. et al. Coenzyme Q10 prevents GDP-sensitive mitochondrial uncoupling, glomerular hyperfiltration and proteinuria in kidneys from db/db mice as a model of type 2 diabetes. *Diabetologia* **55**, 1535–1543 (2012).
- Wong, B. W., Marsch, E., Treps, L., Baes, M. & Carmeliet, P. Endothelial cell metabolism in health and disease: impact of hypoxia. *EMBO J.* **36**, 2187–2203 (2017).
- Osuma, E. A., Riggs, D. W., Gibb, A. A. & Hill, B. G. High throughput measurement of metabolism in planarians reveals activation of glycolysis during regeneration. *Regeneration* **5**, 78–86 (2018).
- Magadam, A. & Engel, F. B. PPAR $\beta$ /delta: linking metabolism to regeneration. *Int. J. Mol. Sci.* **19**, 2013 (2018).
- Zheng, X. et al. Triggering of a Dll4-Notch1 loop impairs wound healing in diabetes. *Proc. Natl Acad. Sci. USA* **116**, 6985–6994 (2019).
- Li, X. et al. MicroRNA-132 with therapeutic potential in chronic wounds. *J. Invest. Dermatol.* **137**, 2630–2638 (2017).

### Acknowledgements

This work was supported by grants from the Swedish Research Council, Stockholm County Research Council, Stockholm Regional Research Foundation, Bert von Kantzows Foundation, Swedish Society of Medicine, Konung Gustaf V:s och Drottning Victrias Frimurarestifelse, Karolinska Institute's Research Foundations, and Strategic Research Programme in Diabetes. We thank Irène Gallais Sérézal, Peter Berg, Fredrik Correa, Martin Gumulka, Mahsa Tayefi, and Ola Rollman for biopsy collection from venous ulcers.

### Author contributions

S.N., X.Z. and S.-B.C. devised hypotheses and designed the experiments. S.N., S.E.A., C.X., J.G., A.Z., W.Z., I.R.B., N.R.E. and X.Z. performed experiments and collected the



data. N.X.L., M.S., J.Z., M.I., and S.-B.C. provided resources and funding supports. S.N., X.Z., R.G.M. and S.-B.C. wrote the manuscript. S.N., S.E.A., C.X., J.G., A.Z., W.Z., N.X.L., M.S., J.Z., M.I., R.G.M., I.R.B., N.R.E., X.Z. and S.-B.C. contributed to the discussion, revision, proofing and approval of the preliminary and revised manuscripts.

### Funding

Open Access funding provided by Karolinska Institute.

### Competing interests

The authors declare no competing interests.

### Additional information

**Supplementary information** is available for this paper at <https://doi.org/10.1038/s42003-020-01495-y>.

**Correspondence** and requests for materials should be addressed to X.Z. or S.-B.C.

**Reprints and permission information** is available at <http://www.nature.com/reprints>

**Publisher's note** Springer Nature remains neutral with regard to jurisdictional claims in published maps and institutional affiliations.



**Open Access** This article is licensed under a Creative Commons Attribution 4.0 International License, which permits use, sharing, adaptation, distribution and reproduction in any medium or format, as long as you give appropriate credit to the original author(s) and the source, provide a link to the Creative Commons license, and indicate if changes were made. The images or other third party material in this article are included in the article's Creative Commons license, unless indicated otherwise in a credit line to the material. If material is not included in the article's Creative Commons license and your intended use is not permitted by statutory regulation or exceeds the permitted use, you will need to obtain permission directly from the copyright holder. To view a copy of this license, visit <http://creativecommons.org/licenses/by/4.0/>.

© The Author(s) 2020